Trade-off between power extraction maximisation and fatigue reduction in wind farms via second-order sliding mode control and min–max optimisation

IET Journals
The Institution of Engineering and Technology

Trade-off between Power Extraction Maximization and Fatigue Reduction in Wind Farms via Second Order Sliding Mode Control and Minimax Optimization

ISSN 1751-8644
doi: 0000000000
www.ietdl.org

E. Capello[1,*], *T. Wada*[2], *E. Punta*[3], *Y. Fujisaki*[2]

[1] *Department of Mechanical and Aerospace Engineering, Politecnico di Torino, and with Institute of Electronics, Computer and Telecommunication Engineering, National Research Council of Italy (CNR-IEIIT), Torino, Italy*
[2] *Department of Information and Physical Sciences, Osaka University, Suita, Japan*
[3] *Institute of Electronics, Computer and Telecommunication Engineering, National Research Council of Italy (CNR-IEIIT), Torino, Italy*
✉ *E-mail: elisa.capello@polito.it*

Abstract: In the last ten years, with the increase of renewable energies, great attention is devoted to operation and maintenance of wind turbines and wind farms, which are the fundamental objectives to be guaranteed by the design of control systems. This paper proposes a trade-off approach between fatigue reduction and power extraction for wind farm scenarios. The focus of this approach is to reduce maintenance costs for fatigue loads. This issue is solved by an optimization problem, in which the maximum fatigue load among the turbines in the wind farm is minimized, then pitch angle and tip-speed ratio are given as reference points for each turbine in the wind farm. Furthermore, the super-twisting sliding mode algorithm is used for the rotor speed control and it shows that the turbines work at the optimized operating points. Moreover, the sliding mode controller produces continuous torques and improves the wind turbine performance by enhancing energy capture and reducing dynamic loads. The effectiveness of the method is illustrated through simulations of two wind farm scenarios. The results obtained with the proposed approach are compared with the case when each turbine in the wind farm tracks the maximum power operating point.

1 Introduction

Wind power is projected to become the most significant source of renewable energy, considering that world wind power generation has increased more than ten times in the last ten years [1]. As clearly explained in [2, 3], advanced control methods are able to improve wind power technologies through several aspects including the mitigation of fatigue loads. Moreover, as in [3], since several subsystems are involved in a wind farm scenario, the main objectives of control systems can be divided in three categories: (i) maximizing captured power from wind, (ii) alleviating fatigue loads on wind turbines, and (iii) improving output power quality. The key feature of the proposed research is the combination of advanced control techniques and of an optimization approach, to have a trade-off between power extraction maximization and fatigue reduction.

The cost of wind power generation is largely determined by the costs of the turbine components and therefore by the wear of the components due to mechanical loads; the use of advanced control algorithms directly affects costs by reducing loads [4, 5]. Moreover, as the size of wind turbines is increased in the past years, the demands on control systems are increased on reduction the structural loads. Our main control objective is related to "power" smoothing [6] and reduction of the mechanical fatigue through an "advanced" control system based on theory of sliding mode control (SMC), with a focus on Region 2 [3, 7] of wind turbine operations.

A wind farm is an array of wind turbines installed in the same area and used to produce electricity. Turbines are often sited together in wind farms as it is economically advantageous [8]. However, in wind farm scenario, turbines are subject to reduced wind speed due to wake interactions and increased turbulence, leading to a reduced energy extraction and increased dynamic mechanical loads on the turbine, respectively. Indeed, the wind turbines extract a part of energy from the wind flow which causes decrease in wind speed behind them, introducing a speed deficit behind wind turbines, usually called wake. Moreover, currently, the wind farms are typically composed of a large number of wind turbines on a relatively small area, which causes the turbines to share the common energy resource.

Traditionally, a wind farm is operated as a collection of individually controlled wind turbines [9], which is not necessarily production-wise the best operating strategy for a large number of closely-spaced turbines. When a wind turbine is individually controlled, it usually works at its locally optimal operating point which assures it extracts the maximum available power from the wind at its rotor. The control strategy which is called maximum power point tracking (MPPT) leads to maximize captured power when wind speed is below its rated value. In literature, different control algorithms are proposed to maximize the power and to track the variable angular velocity, starting from Proportional Integrative Derivative (PID) output feedback control [10, 11] to adaptive control [12, 13]. However, due to the aerodynamic interaction, the MPPT strategy of each turbine does not lead to maximal total power capture across the entire wind farm. Usually, the turbines on the upwind side of the farm extract too much power, slowing the wind too much before it reaches other turbines on the farm [7]. This means that the efficiency of the wind power conversion systems can be greatly improved by using an appropriate control algorithm. As detailed in [14], one important specification in the wind systems is to mitigate loads in the turbine components to increase their life time and reduce the maintenance. This can be done adopting different approaches: (i) through advanced components mechanical design, (ii) through the introduction of new materials or (iii) by improving the control itself. In [15], combined control of the pitch blade is proposed to reduce the dynamic loads acting on the system. However, this work is limited to load reduction without any evaluation of the power extraction. Moreover, as in [16], in which a survey of advanced control techniques for power capture is presented, understanding the dynamics and modeling of complex wind turbine systems is important for analyzing the control objectives and synthesizing the control algorithms. Instead,

as said before, the main focus of our paper is to improve the control design in Region 2, combining it with an optimization problem and a wave model, trying to improve the power extraction.

In the last few years, different control schemes based on the theory of sliding mode control (SMC) are presented for wind turbines, also using super-twisting (STW) SMC strategies [17, 18]. In [19], an adaptive robust sliding mode control for a variable speed wind power generation is described. A robust aerodynamic torque observer is also designed in order to avoid the wind speed sensors. Another adaptive robust control law [17] based on a sliding mode control theory achieves good performance under system uncertainties. Recently, a sliding mode controller for the tracking of the MPPT operating point is proposed [20], in which the effectiveness of the control strategy in wind energy conversion system is proven with direct-driven in permanent magnet synchronous generator. In a similar way, in [21] the effectiveness of a robust sliding mode controller is verified with a single turbine, including doubly-fed induction generator (DFIG) model.

In our paper, a STW SMC [22] is selected to guarantee high efficiency and robustness to parametric uncertainties. Moreover, the STW sliding mode approach leads to a continuous torque, thus reducing the chattering phenomenon and therefore the mechanical stress since no large torque variations are generated. As already explained, for a single turbine, the aim of control algorithms in modern wind turbines are to adjust the control degrees of freedom of the turbine, with the aim of maximizing the energy capture of the wind turbine while keeping the structural loads on the turbine within acceptable limits. In this case, the STW controller acts on the generator angular velocity to reach the maximum extraction of power, starting from operating conditions obtained with an optimization problem. Thus, the scope of the optimization problem is to minimize the aerodynamic interference between the turbine and to maximize the overall power reducing the fatigue loads.

For giving operating points among wind turbines, we provide an optimization problem which is to minimize the maximum fatigue load among wind turbines. We can fairly allocate fatigue loads to them via this optimization. Notice that, if the total fatigue loads in a wind farm is minimized, fatigue loads of some specific wind turbines may become large. In this case, we have to select short maintenance interval to avoid outage of them. On the contrary, since the minimax optimization minimizes the maximum fatigue loads and its allocation could lead to a long maintenance interval. Then, it is efficient to reduce maintenance cost. As said, placing wind turbines in a wind farm introduces aerodynamic interaction among the turbines that affect power production and load on each turbine in the farm. These interaction effects are usually not taken into account in the current practice of wind turbine control design. The novelty of our paper is to obtain the maximum power for a coordinated wind farm, considering the interaction between the power production and the loads of each turbine in the farm. Pre-defined configurations of the wind turbines are selected for the optimization problem. In our paper, the main focus is related to the combination of two algorithms: (i) one for the evaluation of operating points in which the power is maximized and the maximum loads among turbines are minimized and (ii) one control system able to track the desired operating points. Instead, for example, in [23] the main focus is the definition of a novel method for wind farm layout optimization based on wind turbine selection, that is the power is optimized, in function of the wind farm layout. In a similar way, in [24] an optimization algorithm for the definition of the wind farm layout is proposed. In our paper, the proposed "advanced" control law can be combined with the optimization problem, to define a trade-off between the maximum energy and the minimum fatigue loads, guaranteeing a reduction of the maintenance costs. The optimization problem is not focused on the definition of the wind farm layout, but is focused on the definition of desired operating points. Finally, our challenging task is to achieve good load reduction without compromising energy capture performance.

This work is based on our previous researches described in [25, 26]. The contribution of this work with respect to these previous works are: (i) evaluation of wind variations including Jensen wake model [5, 27], (ii) trade-off between fatigue loads and power optimization to reduce the maintenance costs, and (iii) comparison with MPPT operating point to demonstrate the reduction of fatigue, even in presence of power extraction reduction. Finally, the proposed optimization problem focus on finding operating points, that guarantee the trade-off between the power extraction and the load reduction.

The paper is organized as follows. The overview of main features of a wind farm and the model of a wind farm is introduced in 2. In the same section, a dynamical model of a single wind turbine is presented. Moreover, wake interactions are analyzed in Section 2.3 by Jensen model. In Section 3, a min-max optimization problem is defined for evaluation of operating points. Section 4 proposes a STW sliding mode controller suitably designed for tracking the desired operating points. Some preliminary results for two wind farm scenarios are presented in 5 including aerodynamic interference and comparison with the maximum power point tracking. Finally, some concluding remarks are described in Section 6.

2 Wind Farm Scenario

As described in [7], there are three main operating regions for a variable speed wind turbine, regardless of whether it operates alone or in a wind farm. Region 1 concerns the starting mode of the turbine operation. Region 2 is the operation mode during which the turbine captures the most power possible from the wind. Region 3 is when the wind speed is enough high to allow the turbine to limit the fraction of the captured wind power, so as not to exceed the safe electrical and mechanical loads.

In this paper, the focus is on Region 2 which corresponds to the operation mode at variable speed/optimum tip-speed ratio [28].

2.1 Wind Turbine Model

In this paper, it is assumed that the wind speed is approximately between 5 and 14 m/s, that the blade pitch is set at a constant optimum value for the peak energy extraction, and that each wind turbine is operating in Region 2. The considered wind turbine model is simplified by considering negligible external stiffness [29].

The dynamics of the rotor of a wind turbine can be written as

$$\dot{\omega}_r = \frac{T_a}{J_t} - \frac{K_t}{J_t}\omega_r - \frac{T_g}{J_t}, \tag{1}$$

where ω_r is the rotor speed, T_a and T_g are the aerodynamic and the generator torques, respectively. The aerodynamic torque is given by wind drives the wind turbine at an angular speed ω_r, which is increased by a gearbox ratio $n_g = \omega_g/\omega_r$ to obtain the generator speed ω_g. The generator torques T_g, which is determined by generator electromagnetic torque, is control input of the above system. The coefficient K_t is combination of the rotor and generator external damping, that is, $K_t = K_r + n_g^2 K_g$. In a similar way, the moment of inertia $J_t = J_r + n_g^2 J_g$ is combination of the rotor and generator moment of inertia. See [18] for more details. All the symbols are in Fig. 1.

The aerodynamic torque T_a is defined via the torque coefficient C_T such as

$$T_a = \frac{1}{2}\rho\pi R^3 C_T(\lambda,\beta)w^2, \tag{2}$$

where ρ is the air density, R is the radius of the circumference traced by the tips of the wind turbine blades, and w is the wind speed. The torque coefficient $C_T(\lambda,\beta)$ in (2) is a function of the blade tip-speed ratio λ and of the blade pitch angle β. The tip-speed ratio is in general the ratio between the tangential speed of the tip of a blade and the wind speed which is defined as

$$\lambda = \frac{R\omega_r}{w}. \tag{3}$$

In our case, the pitch angle is set at a constant optimal value for energy extraction for all the considered scenarios.

As for the measure of the wind speed w, generally, in traditional wind turbine, an anemometer is placed on the upper part of the

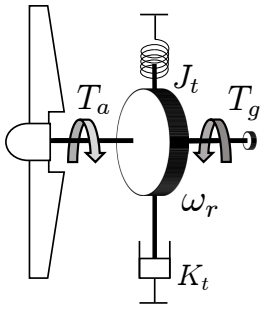

Fig. 1: Wind turbine dynamics

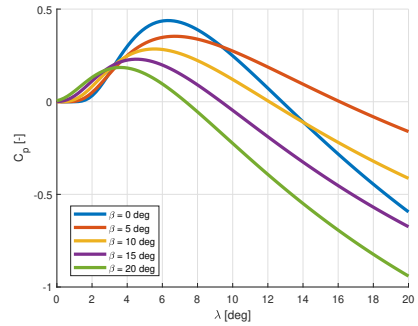

Fig. 2: Variation of the power coefficient with λ and β

nacelle. Here we consider a more recent measurement technology based on light detection and ranging (LIDAR) sensor [30, 31]. This sensor is able to measure wind speed over a distance of hundreds of meters, therefore information on incoming wind speed are available and can be included in the turbine control system.

For any specific wind turbine, the power coefficient C_P is a measure of wind turbine efficiency which is often used by wind power industries. In fact, it is defined as the ratio of actual electric power produced by a wind turbine divided by the total wind power flowing into the turbine blades at specific wind speed. The power coefficient C_P can be defined as a function of λ and β as follows

$$C_P(\lambda,\beta) = c_1\left(\frac{c_2}{\bar{\lambda}} - c_3\beta - c_4\right)e^{\frac{-c_5}{\bar{\lambda}}}, \quad (4)$$

$$\frac{1}{\bar{\lambda}} = \frac{1}{\lambda + 0.08\beta} - \frac{0.035}{\beta^3 + 1}, \quad (5)$$

where the angles are expressed in degrees [32, 33] and the coefficients $c_1, c_2, \ldots, c_5$ depend on the specific wind turbine. In a practical situation, the power coefficient C_P for a particular turbine is measured or calculated by the manufacturer, and usually provided at various wind speeds such as Fig. 2.

The aerodynamic power P_a and the generator power P_g can be evaluated from the torque

$$P_a = T_a\omega_r, \qquad P_g = T_g\omega_r.$$

For the wind turbine control problem, the optimal operating point is evaluated from the maximum angular rotation speed ω_{opt},

$$\omega_{\text{opt}} = \frac{\lambda_{\text{opt}} w}{R}, \quad (6)$$

where λ_{opt} is obtained by either (i) the peak of power coefficient, if the MPPT tracking is analyzed or (ii) the output of an optimization problem (described in Section 3). For both cases, the pitch angle β is considered as a constant. A variable wind speed behavior is included in the model starting from the model described in [34] and including random noise.

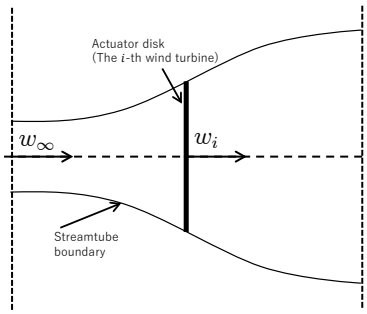

Fig. 3: Actuator disk theory and speed variation

2.2 *Wind Farm Model*

As briefly introduced earlier, wind farms are composed of a number of wind turbines, usually located on a relatively small area. Each wind turbine extracts a part of the energy from the wind flow; this causes decrease in wind speed after the turbine and introduces aerodynamic interactions and wind speed deficits for subsequent turbines.

For a wind farm scenario, the total power generation $P_{g,i}$ of each turbine should be easily written in function of the axial induction factor a_i as

$$P_{g,i} = \frac{1}{2}\rho\pi R^2 w_i^3 a_i(1-a_i)^2,$$

in which w_i is the wind speed acting on the i-th wind turbine, affected by the aerodynamic interactions (see Section 2.3). The axial induction factor a_i is defined as the velocity reduction relative to the free wind speed and it is obtained starting from the actuator disk model [35] (see Fig. 3) as

$$a_i = \frac{w_\infty - w_i}{w_\infty}, \quad (7)$$

where w_∞ is the wind speed not affected by aerodynamic interactions and w_i is the speed acting on the i-th turbine.

From the axial induction factor definition, the power and torque coefficients are respectively the percentage of power extracted by the wind turbine from the wind resource and the torque acting on the turbine. These coefficients are evaluated starting from the actuator disk theory [36, 37] as follows

$$C_{P,i} = 4a_i(1-a_i)^2, \quad (8)$$

$$C_{T,i} = 4a_i(1-a_i). \quad (9)$$

The speed w_i is function of the speed acting on the first turbine (i.e. the flow speed w_∞) and it is affected by aerodynamic interactions (deeply discussed in Section 2.3).

The main idea of the energy extraction from the wind is caused by the capture of the kinetic energy from the wind, that is limited by the Betz law (well defined in [38]). This law defines the maximum value for the power coefficient C_P, to which corresponds a maximum value for the axial induction factor. We have that $C_{P,\max} = 16/27 \approx 0.59$ and $a_{\max} = 1/3$. This equation can be translated in

$$C_{P,i} = 4a_i(1-a_i)^2 = \frac{P_{\text{mech},i}}{P_{\text{wind},i}}, \quad (10)$$

where $P_{\text{wind},i}$ is the maximum power extracted from the i-th wind turbine and $P_{\text{mech},i}$ is the mechanical power, that cannot be more than 59% of $P_{\text{wind},i}$. In real applications, this value is reduced due to unmodeled dynamics and energy losses in the actuator disk model. Notice that the values of the coefficients (4) depends on the wind turbine design, that is, λ and β are control parameters for speed regulation and power production.

Since the wind perturbation could lead to outage of a wind turbine, intensity of turbulence effect at i-th wind turbine is modeled

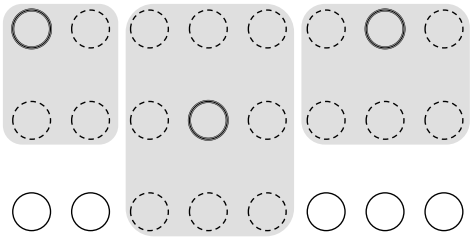

Fig. 4: The schematic representation of the wind turbines in a wind farm is shown. Each circle corresponds to a wind turbine. The circle in bold indicates the turbine considered in each case. Three instances of proximity may occur (three corresponding gray areas): (a) the turbine considered is in a corner position of the wind farm and, consequently, has three turbines nearby; (b) the turbine considered is located in a position inside the wind farm and, consequently, has eight turbines nearby; (c) the turbine considered is in a position on the border of the wind farm and, consequently, has five turbines nearby.

[39, 40] as

$$I_{\text{eff},i}(w_i) = \left(\int_0^{2\pi} p(\theta \mid w_i)(I_i(\theta \mid w_i))^m \mathrm{d}\theta \right)^{1/m},$$

where $I_{\text{eff},i}$ is effective turbulence intensity which corresponds to fatigue risk of the wind turbine, p is a probability density function of wind direction for a given wind speed w_i, θ is wind direction, I_i is turbulence intensity combined of ambient and wake flow from wind direction, and m is Wõhler exponent which depends on material of blades of the wind turbine.

We assume that θ is the wind direction and the uniform random variable on $[0, 2\pi]$, p is its probability density function, the wind turbines in a row are arranged at the same interval ℓ_r, and those in a column are equally spaced and its distance is ℓ_f. Under the above assumptions, effective turbulence intensity at the i-th wind turbine is given by

$$I_{\text{eff},i}(w_i) = \begin{cases} \dfrac{\hat{\sigma}}{w_i} & \text{if } \min\{\ell_r, \ell_f\} \geq 20R \\ \dfrac{\hat{\sigma}_{\text{eff},i}}{w_i} & \text{if } \min\{\ell_r, \ell_f\} < 20R \end{cases} \tag{11}$$

where $\hat{\sigma}$ is a characteristic ambient turbulence standard deviation,

$$\hat{\sigma}_{\text{eff},i} = \left((1 - 0.06|\mathcal{N}_i|)\hat{\sigma}^m + 0.06 \sum_{j \in \mathcal{N}_i} \hat{\sigma}_T^m \right)^{1/m},$$

$\mathcal{N}_i$ is the set of wind turbines which are neighbor of the i-th wind turbine (see Fig. 4 for detail), $\hat{\sigma}_T$ is the standard deviation of the maximum center-wake turbulence at the hub height. Finally,

$$\hat{\sigma}_T = \sqrt{\frac{w_i^2}{\left(1.5 + \dfrac{0.4\ell_{ij}}{R\sqrt{C_{T,j}}}\right)^2} + \hat{\sigma}^2},$$

where ℓ_{ij} is distance between the i-th and j-th wind turbine in blade diameters, and $C_{T,j}$ is the torque coefficient of the j-th wind turbine.

The turbulence effect cannot be described by means of the actuator disk model in its standard form due to the many ideal hypothesis assumed. For this reason, we use the polynomial approximation proposed by [41], in which the fatigue damage is modeled as

$$D_i = c w_i^2 I_{\text{eff},i}^2 (z_2 a_i^2 + z_1 a_i + z_0), \tag{12}$$

where w_i is the wind speed acting on the i-th turbine, I_{eff} is defined in Eq. (11), and $c = 1$. The polynomial coefficients are obtained from [41] such as $z_2 = 127.5$, $z_1 = -12.41$ and $z_0 = 4.65$. The wind speed variation is evaluated including the aerodynamic interactions, that will be described in the next section. In a similar way, the fatigue can be defined as a function of the axial induction factor and the wind speed,

$$F_i = 2\rho A_0 (4a_i(1 - a_i)) w_i^2, \tag{13}$$

where $A_0 = \pi R^2$ is the disk area of the i-th turbine, a_i is the axial induction factor of the i-th turbine and w_i is the wind speed acting on the i-th turbine, as before.

2.3 Jensen Model

The wake model chosen for this research is known as Jensen/Park model, developed in the 1980s by N.O. Jensen [5]. This model is a kinematic, parametric, static model developed starting from the actuator disk model theory [35], see Fig. 3. The main assumptions of this last theory are (i) linear expansion of the wake and (ii) superposition effect of multiple wakes acting on a turbine. Moreover, it is based on the assumption of a wake with linearly expanding diameter.

Starting from definition of the power and torque coefficients (9) can be derived that

$$1 - 2a_i = \sqrt{1 - C_{T,i}}, \tag{14}$$

where a_i and $C_{T,i}$ are the axial induction factor and the torque coefficient of the i-th turbine, respectively. Assuming a linear expansion, the linear dimension (radius R) is proportional to the down-wind distance x, as in the following equation

$$R(x) = R + \alpha x. \tag{15}$$

As explained in [42], α is defined as the decay coefficient and it is set to 0.075 for onshore, and to 0.05 for offshore wind farms, see Fig. 5 in which $R(x)$ is defined.

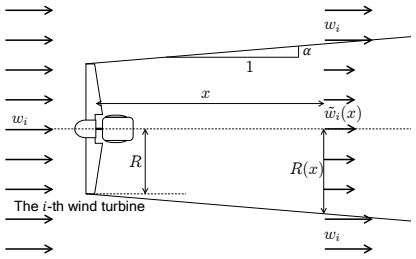

Fig. 5: Linear expansion of the wake assumed in Jensen wake model [42]

The wind speed in the wake at distance x from the turbine can be computed as

$$\tilde{w}_i(x) = w_i \left[1 - (1 - \sqrt{1 - C_{T,i}}) \left(\frac{R}{R(x)} \right)^2 \right]. \tag{16}$$

The wind speed is function of the wind speed not affected by the wake model w_i and of the radius $R(x)$.

In Equation (16), the effects of multiple wakes or a partial shadowing of the turbines are not included. Moreover, in our case, we assume that all the considered turbines have the same radius. With this assumption, the shadowing area can be defined as the intersection between the area of the input wake of a specific turbine and the circular area of this turbine. According to the paper [42], we consider four cases, that is, no shadowing case, partial shadowing case, quasi-complete shadowing case, and complete shadowing case. In no shadowing case (Fig. 6 (a)), there is no overlapping region between the input wake and the circular area of the turbine. The complete shadowing case (Fig. 6 (d)) means that the input wake area completely includes the circular area. Between two cases, there are

partial shadowing case, quasi-complete shadowing case. In quasi-complete shadowing case (Fig. 6 (c)), the center of the circular area of the turbine is inside of the wake stream area. The other case is the partial shadowing (Fig. 6 (b)). The region corresponds to the hatched one in Fig. 6. The area $A_{sh,ij}$ is zero if the turbine i is behind of the turbine j. Otherwise, the area for each case is given by

$$A_{sh,ij} = \begin{cases} 0 & \text{if } d_{ij} \geq R(x_{ij}) + R \\ R^2(x_{ij})\theta_x + R^2\theta - d_{ij}z_{ij} & \text{if } R(x_{ij}) + R > d_{ij} \geq R(x_{ij}) \\ R^2\theta - \dfrac{Rz_{ij}}{2}\cos\theta & \\ \quad + R^2(x_{ij})\theta_x - \dfrac{R(x_{ij})z_{ij}}{2}\cos\theta_x & \text{if } R(x_{ij}) > d_{ij} \geq R(x_{ij}) - R \\ R^2\pi & \text{if } d_{ij} < R(x_{ij}) - R \\ 0 & \text{if the turbine } i \text{ is behind } j \end{cases} \quad (17)$$

where the distance d_{ij} is the x-axis relative distance between the turbines i and j and

$$z_{ij} = \begin{cases} 2R(x_{ij})\sin\theta_x & \text{if } R(x_{ij}) + R > d_{ij} \geq R(x_{ij}) \\ 2R\sin\theta & \text{if } R(x_{ij}) > d_{ij} \geq R(x_{ij}) - R \end{cases}$$

$$\theta_x = \cos^{-1}\left(\frac{R^2(x_{ij}) + d_{ij}^2 - R^2}{2d_{ij}R(x_{ij})}\right) \quad \text{if } R(x_{ij}) + R > d_{ij} \geq R(x_{ij}) - R,$$

$$\theta = \cos^{-1}\left(-\frac{R^2(x_{ij}) - d_{ij}^2 - R^2}{2d_{ij}R}\right) \quad \text{if } R(x_{ij}) + R > d_{ij} \geq R(x_{ij}) - R.$$

For all the details refer to [42].

Applying the superposition effect, the complete model for the input wind speed of a turbine is

$$w_i = w_\infty \left[1 - (1 - \sqrt{1 - C_{T,i}}) \sum_{j=1, j\neq i}^{n} \left(\frac{R}{R(x_{ij})}\right)^2 \frac{A_{sh,ij}}{A_0}\right]. \quad (18)$$

This shadowing is a measure of the degree of overlap between the area defined by the wakes shadow cone ($A_{sh,ij}$) and the area swept by the turbine experiencing shadowing ($A_0 = \pi R^2$), as in Fig. 6.

In our systems, the number of wind turbines and the layout of the wind farm are known, so the wake interactions between turbines are known a priori. Two simulation scenarios are considered in Section 5, for both of them we assume $w_1 = w_\infty$, since the first turbine is not affected by wake interaction.

3 Energy Optimization with Fatigue Constraints

We have already seen that, if wind turbines are placed very closely each other, interference among them gives rise to stress on turbine blades. This additional stress could cause an extra maintenance cost. On the other hand, although this cost may be reduced by placing wind turbines sparsely, a larger area is needed in this case and thus a great cost is required for wind farm construction. From this point of view, our goal is to find preferable operating points of wind turbines, which may be placed densely. Notice here that the effective turbulence intensity $I_{\text{eff},i}$ corresponds to the fatigue risk. In the following, we consider minimization of maximum effective turbulence intensity $I_{\text{eff},i}$ in the wind farm. This minimax formulation enables us to realize fatigue risk balancing over the wind turbines of the farm, which is in fact preferable since the maintenance intervals of the turbines can be balanced.

Our problem is to minimize the maximum among the effective turbulence intensity $I_{\text{eff},i}$, $i = 1, 2, \ldots, n$ in a wind farm subject to a constraint on power generation, that is,

$$\min \max_{i=1,2,\ldots,n} \quad I_{\text{eff},i} \quad (19)$$

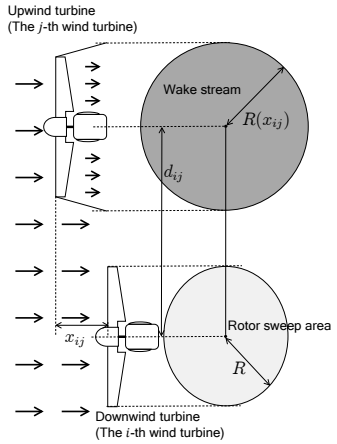

(a) No shadowing ($d_{ij} \geq R(x_{ij}) + R$)

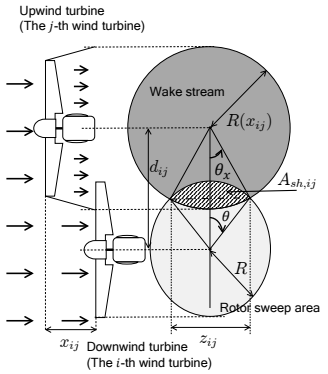

(b) Partial shadowing ($R(x_{ij}) + R > d_{ij} \geq R(x_{ij})$)

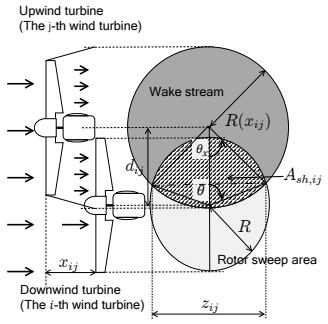

(c) Quasi-complete shadowing ($R(x_{ij}) > d_{ij} \geq R(x_{ij}) - R$)

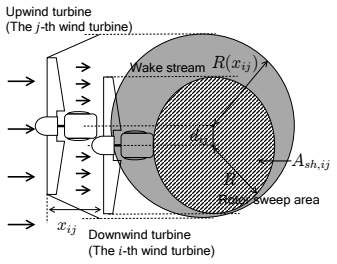

(d) Complete shadowing ($d_{ij} < R(x_{ij}) - R$)

Fig. 6: Effect and parameters of partial shadowing [42]

$$\text{s.t.} \qquad \sum_{i=1}^{n} P_{g,i} = P_{\mathrm{d}},$$

where $P_d \in \mathbb{R}$ is demand power. In our scenario, the owner of the wind farm makes a contract which he sells power P_d. Thus, the contract requires us to generate P_d in this wind farm.

Our control variables in the effective turbulence intensity $I_{\mathrm{eff},i}$ of the i-th wind turbine are the torque coefficients $C_{T,i}$ and $C_{T,j}$ of i-th wind turbine and its neighborhoods $j \in \mathcal{N}_i$ of the i-th wind turbine. On the contrary, active power generation $P_{g,i}$ depends on the power coefficient $C_{P,i}$ of the i-th wind turbine. However, the torque coefficients $C_{T,i}$ and the power coefficient $C_{P,i}$ are not independent variable. Thus, we do not select $C_{T,i}$ and $C_{P,i}$, $i = 1, 2, \ldots, n$ as decision variables in our optimization problem. Since both variables are characterized by the axial induction factor $a_i \in [0, a_{\max}]$ such as

$$C_{P,i} = 4a_i(1 - a_i)^2, \quad C_{T,i} = 4a_i(1 - a_i),$$

the axial induction factors a_i , $i = 1, 2, \ldots, n$ are control variables in our problem.

On the other hand, notice that we cannot control a characteristic ambient turbulence standard deviation $\hat{\sigma}$ which is contained in the definition of the effective turbulence intensity

$$I_{\mathrm{eff},i} = \frac{\hat{\sigma}_{\mathrm{eff},i}}{w_i} = \left((1 - 0.06|\mathcal{N}_i|) \frac{\hat{\sigma}}{w_i}^m + 0.06 \sum_{j \in \mathcal{N}_i} \left(\frac{\hat{\sigma}_{T,i}}{w_i} \right)^m \right)^{1/m}.$$

The ambient turbulence standard deviation $\hat{\sigma}$ is evaluated starting from the method proposed in [27, 40]. Thus, when we solve the optimization, we can neglect its first term.

Now, let us ignore the first term of the effective turbulence intensity. This is because the first term is constant. By introducing an upper bound $\bar{\varepsilon}$ of the second term in Eq. (3) among all of the turbines $i = 1, 2, \ldots, n$, we formulate a minimization problem instead of the minimax optimization (19):

$$\begin{aligned} \min_{a_1, a_2, \ldots, a_n, \bar{\varepsilon}} \quad & \bar{\varepsilon} \qquad (20) \\ \text{s.t.} \quad & \sum_{i=1}^{n} P_{g,i} = P_{\mathrm{d}} \\ & \sum_{j \in \mathcal{N}_i} \left(\frac{1}{\left(1.5 + \frac{0.4\ell_{ij}}{R\sqrt{C_{T,j}}} \right)^2} + \left(\frac{\hat{\sigma}}{w_i} \right)^2 \right)^{m/2} \leq \bar{\varepsilon} \\ & 0 \leq a_i \leq a_{\mathrm{mppt}} \\ & P_{g,i} = \frac{1}{2} \rho \pi R^2 w_i^3 a_i (1 - a_i)^2, \qquad i = 1, 2, \ldots, n, \end{aligned}$$

where the i-th torque coefficient $C_{T,i}$ is $4a_i(1 - a_i)$ and a_{mppt} is a scalar satisfying

$$4a(1 - a)^2 = \max_{\lambda, \beta} C_P(\lambda, \beta), \quad 0 \leq a \leq a_{\max}.$$

Notice that there is a gap between a power coefficient $C_{P,i} = 4a_i(1 - a_i)^2$ which is defined by actuator disk theory and a practical power coefficient (4). To avoid this issue, we consider the constraint $a_i \leq a_{\mathrm{mppt}}$. Just as a reminder, $a_{max} \neq a_{\mathrm{mppt}}$.

Moreover, we have two scenarios on the wind speed w_i, that is included in the optimization problem. The former scenario is that we can measure or predict average wind speed at each wind turbine with high accuracy. That is, wind speed w_i is considered fixed. The latter case is that we know the wind speed affecting the first turbine (i.e. $w_1 = w_\infty$) only. Then, we suppose that wind speeds at other turbines are according to Jensen model and we solve the problem:

$$\begin{aligned} \min_{a_1, a_2, \ldots, a_n, \bar{\varepsilon}} \quad & \bar{\varepsilon} \qquad (21) \\ \text{s.t.} \quad & \sum_{i=1}^{n} P_{g,i} = P_{\mathrm{d}} \\ & \sum_{j \in \mathcal{N}_i} \left(\frac{1}{\left(1.5 + \frac{0.4\ell_{ij}}{R\sqrt{C_{T,j}}} \right)^2} + \left(\frac{\hat{\sigma}}{w_i} \right)^2 \right)^{m/2} \leq \bar{\varepsilon} \\ & 0 \leq a_i \leq a_{\mathrm{mppt}} \\ & P_{g,i} = \frac{1}{2} \rho \pi R^2 w_i^3 a_i (1 - a_i)^2 \\ & w_i = w_\infty \left[1 - 2a_i \sum_{j=1, j \neq i}^{n} \left(\frac{R}{R(x_{ji})} \right)^2 \frac{A_{sh,ji}}{A_0} \right] \\ & i = 1, 2, \ldots, n. \end{aligned}$$

Notice that, in the problem (21), wind speed is not constant and depends on its own axial induction factor a_i.

Both optimization problems are nonconvex due to their constraints. However, we can find a local optimal solution by using some standard solvers, for example, we can use fmincon function [43, 44] in Optimization Toolbox of MATLAB.

After solving the above optimization problems, we need to find physical control variables, that is, a reference tip-speed ratio λ_i and a reference pitch angle β_i. We employ these values for control of each wind turbine. To find a reference tip-speed ratio λ_i and a reference pitch angle β_i, we solve

$$C_P(\lambda_i, \beta_i) = 4a_i(1 - a_i)^2 \qquad (22)$$

with respect to λ_i and β_i for each $i = 1, 2, \ldots n$. From Fig. 2, we see that there exist multiple solutions λ_i and β_i according to Equation (22). However, it is not difficult to find one solution. For example, if we give $a_i = 0.2$, we can find a solution $(\lambda_i, \beta_i) = (6.2073, 0.0000)$.

Remark 1. *If we need to maximize generation power under fatigue constraints, we consider the following problem*

$$\begin{aligned} \max_{a_1, a_2, \ldots, a_N} \quad & \sum_{i=1}^{n} P_{g,i} \\ \textit{s.t.} \quad & \sum_{j \in \mathcal{N}_i} \left(\frac{1}{\left(1.5 + \frac{0.4\ell_{ij}}{R\sqrt{C_{T,j}}} \right)^2} + \left(\frac{\hat{\sigma}}{w_i} \right)^2 \right)^{m/2} \leq \bar{\varepsilon} \\ & 0 \leq a_i \leq a_{\mathrm{mppt}} \\ & P_{g,i} = \frac{1}{2} \rho \pi R^2 w_i^3 a_i (1 - a_i)^2 \\ & i = 1, 2, \ldots, n. \end{aligned}$$

for given maximum fatigue factor $\varepsilon > 0$ [26].

Example 1. *Let us compare the optimization model* (20) *with MPPT case:*

$$\begin{aligned} \max_{a_1, a_2, \ldots, a_N} \quad & \sum_{i=1}^{n} P_{g,i} \qquad (23) \\ \textit{s.t.} \quad & 0 \leq a_i \leq a_{\mathrm{mppt}} \\ & P_{g,i} = \frac{1}{2} \rho \pi R^2 w_i^3 a_i (1 - a_i)^2 \end{aligned}$$

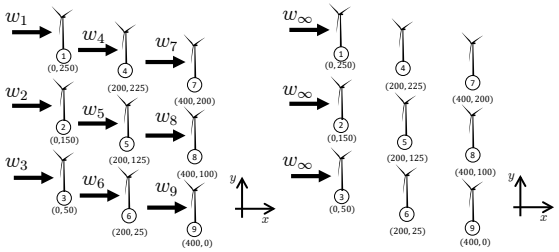

(a) Scenario 1 (b) Scenario 2

Fig. 7: Wind farm setup for the optimization problem

$$i = 1, 2, \ldots, n.$$

As depicted in Fig. 7*, let us consider a wind farm which consists of* 3 *rows. Then, the number of wind turbines in each row is also* 3*. Wind velocity at each wind turbine was selected as*

$$\begin{aligned} w_1 &= 12.0434, \quad w_4 = 10.5784, \quad w_7 = 9.6445 \\ w_2 &= 12.3448, \quad w_5 = 10.3047, \quad w_8 = 9.3416 \\ w_3 &= 12.1707, \quad w_6 = 11.1259, \quad w_9 = 9.3567 \end{aligned}$$

according to uniform random generation from intervals 12 ± 0.5*,* 10.8 ± 0.5*, and* 9.72 ± 0.5 *m/s for each row, where* w_{3i+j}*,* $i = 0, 1, 2$*,* $j = 1, 2, 3$ *corresponds to the induction factor at the* $i+1$*-th row and* j*-th column wind turbine. Air density and rotor diameter were set as* $\rho = 1.2014$ *and* $R = 35$ *m, respectively. The settings of Wõhler exponent* $m = 3$ *and the ambient turbulence standard deviation* $\hat{\sigma} = 0.1$ *were borrowed from them in [27]. Selecting* $P_{\mathrm{d}} = 3.6$ *MW, we solved Problem* (20)*, (local) optimal value was* $\bar{\varepsilon} = 0.0256$ *and (local) optimal solution was*

$$\begin{aligned} a_i &= 0.1525, \quad i = 1, 2, 3, 5, 7, 8, 9 \\ a_4 &= 0.0851, \quad a_6 = 0.1459. \end{aligned}$$

This leads to the effective turbulence intensity as

$$\begin{aligned} &I_{\mathrm{eff},1} = 0.0903, \quad I_{\mathrm{eff},4} = 0.1007, \quad I_{\mathrm{eff},7} = 0.0913, \\ &I_{\mathrm{eff},2} = 0.1127, \quad I_{\mathrm{eff},5} = 0.1153, \quad I_{\mathrm{eff},8} = 0.1130, \\ &I_{\mathrm{eff},3} = 0.0932, \quad I_{\mathrm{eff},6} = 0.1007, \quad I_{\mathrm{eff},9} = 0.0924. \end{aligned}$$

On the other hand, the obtained local optimal value was 3.7462 *MW and the corresponding solution of the problem* (23) *was*

$$a_i = 0.1525, \quad i = 1, 2, \ldots, 9,$$

where a_{3i+j}*,* $i = 0, 1, 2$*,* $j = 1, 2, 3$ *corresponds to the induction factor at the* $i+1$*-th row and* j*-th column wind turbine. Corresponding effective turbulence intensity is*

$$\begin{aligned} &I_{\mathrm{eff},1} = 0.0926, \quad I_{\mathrm{eff},4} = 0.1007, \quad I_{\mathrm{eff},7} = 0.0935, \\ &I_{\mathrm{eff},2} = 0.1141, \quad I_{\mathrm{eff},5} = 0.1216, \quad I_{\mathrm{eff},8} = 0.1142, \\ &I_{\mathrm{eff},3} = 0.0935, \quad I_{\mathrm{eff},6} = 0.1007, \quad I_{\mathrm{eff},9} = 0.0926. \end{aligned}$$

From these results, we see that the maximum effective turbulence intensity of Problem (20) *is lower than that of Problem* (23)*. When we selected more small* P_d*, we can make the maximum effective turbulence intensity small.*

On the other hand, when we consider the second scenario (Fig. 7b*) with* $w_\infty = 12$ *m/s and* $P_d = 4.05$ *MW, we obtained*

$$\begin{aligned} a_1 &= 0.1457, \quad a_4 = 0.0857, \quad a_7 = 0.1280 \\ a_2 &= 0.1525, \quad a_5 = 0.1525, \quad a_8 = 0.1340 \\ a_3 &= 0.1352, \quad a_6 = 0.1013, \quad a_9 = 0.1525 \\ I_{\mathrm{eff},1} &= 0.0903, \quad I_{\mathrm{eff},4} = 0.0995, \quad I_{\mathrm{eff},7} = 0.0887, \\ I_{\mathrm{eff},2} &= 0.1099, \quad I_{\mathrm{eff},5} = 0.1099, \quad I_{\mathrm{eff},8} = 0.1099, \\ I_{\mathrm{eff},3} &= 0.0918, \quad I_{\mathrm{eff},6} = 0.0998, \quad I_{\mathrm{eff},9} = 0.0883. \end{aligned}$$

Since the wind speed at each turbine is different form that of the first scenario, we cannot provide fair comparison among these results. However, we can see that we obtain operating points of a wind farm based on Jensen model even if we can predict w_∞ *only.*

4 Sliding Mode Control for Wind Turbine

Sliding mode is a nonlinear control approach, which is able to ensure high accuracy and excellent robustness against external disturbances and parameter variations with simple design. First order SMCs design discontinuous control laws and guarantee that the sliding manifold is reached (i.e. the sliding output reaches zero), while higher order SMCs can steer to zero the sliding output as well as its higher order time derivatives. The STW algorithm [22] is a second order SMC and is a continuous controller, which is able to provide all the main SMC properties for systems affected by smooth matched uncertainties/disturbances with bounded gradients.

Consider the following uncertain nonlinear control system

$$\dot{x} = f(t, x) + u, \tag{24}$$

where $x \in R$ is the state, $u \in R$ is the control input, and $f(t, x) \in R$ is a possibly uncertain, yet bounded term. The sliding variable $\sigma(t, x) \in R$ is chosen for system (24); σ has relative degree 1 with respect to u. Therefore the dynamics of the sliding output σ can be expressed as follows

$$\dot{\sigma}(t, x) = h(t, x) + u, \tag{25}$$

the uncertain term $h(t, x)$ is assumed bounded as well as its first order time derivative, i.e., $|h(t, x)| < M$ and $|\dot{h}(t, x)| < L$ at least locally.

The relevant sliding surface is defined as follows

$$\sigma(t, x) = 0. \tag{26}$$

The STW control algorithm can be applied to system (24) according to the following

$$\begin{aligned} u &= u_1 + u_2 \\ u_1 &= -k_1 |\sigma|^{\frac{1}{2}} \operatorname{sgn}(\sigma), \\ \dot{u}_2 &= -k_2 \operatorname{sgn}(\sigma), \end{aligned} \tag{27}$$

where σ is the sliding variable in (26) and the two control parameters are chosen such that $k_1 > 1.5L^{\frac{1}{2}}$ and $k_2 > 1.1L$, with $L > 0$ known constant bound of the uncertainty. The STW continuous control law guarantees the convergence of both σ and $\dot{\sigma}$ to zero in a finite time, [22], [45].

In this section we propose the STW SMC strategy for the wind turbine. It is important to note that the presented STW is designed for the control of a wind turbine, which can be either a single wind turbine or any wind turbine in a wind farm. The main control objective is to enhance the captured power and the efficiency, while reducing mechanical fatigue and attenuating the output chattering. The control of the rotor angular speed can improve the performances of a wind turbine by enhancing energy capture and reducing dynamic loads. STW SMC results to be easy to implement, guarantees efficiency and designs a continuous torque for the wind turbine.

The proposed continuous STW SMC is robust to uncertainties of turbine and generator, as well as to electric grid disturbances.

The STW SMC designs a continuous control law for the torque, thus guaranteeing a reduction of the chattering phenomenon. In

fact, no discontinuous torque variations are required, therefore the mechanical stress imposed to the system is greatly attenuated. STW SMC guarantees robustness against matched external disturbances with bounded gradient, and parameter variations. The simplicity in control design is important and must be considered, as well as the quite limited number of signals required by the controller. These facts make the STW particularly well suited to deal with the considered control problem.

Consider the wind turbine (1), whether it operates singularly or in a wind farm. A sliding surface must be appropriately designed to make the wind turbine work at the desired operating point. To this end, we define the following sliding variable

$$\sigma_r = \omega_r - \omega_{\text{opt}}, \tag{28}$$

where ω_r is the rotor angular velocity as previously defined and ω_{opt} is the desired angular velocity to be tracked. The reference ω_{opt} is evaluated to track the defined power point, corresponding to the value λ_{opt}, according to (6). λ_{opt} is obtained as the peak of power coefficient, if the MPPT tracking for a single wind turbine is analyzed (Section 2), or the output of the optimization problem described in Section 3. For both cases, the pitch angle β is considered constant and fixed.

Let us consider the wind turbine (1) and the chosen sliding variable (28), the first order time derivative of σ_r can be expressed as follows

$$\dot{\sigma}_r = \dot{\omega}_r - \dot{\omega}_{\text{opt}} = h_r(t, \omega_r) + g_r T_g, \tag{29}$$

where $h_r(t, \omega_r) = \frac{T_a}{J_t} - \frac{K_t}{J_t}\omega_r - \dot{\omega}_{\text{opt}}$ and $g_r = -\frac{1}{J_t}$.

Assumption 1. *Let us define the operating condition of the wind turbine (1), whether it operates singularly or in a wind farm. Once fixed the considered range for the wind velocities and related first order time derivatives, according to (2)–(6) it is possible to compute constant bounds for the terms $|h_r(t, \omega_r)| < M_r$ and $|\dot{h}_r(t, \omega_r)| < L_r$ at least locally.*

Lemma 1. *Let Assumption 1 hold and consider the wind turbine system (1), the sliding variable (28), and its time derivative (29). The application of the following STW sliding mode controller to the wind turbine (1)*

$$\begin{aligned} T_g &= \frac{1}{g_r}(T_{g1} + T_{g2}), \\ T_{g1} &= -k_{1r}\,|\sigma_r|^{\frac{1}{2}}\, sgn(\sigma_r), \\ \dot{T}_{g2} &= -k_{2r} sgn(\sigma_r), \end{aligned} \tag{30}$$

with control gains chosen as $k_{1r} > 1.5L_r^{\frac{1}{2}}$ and $k_{2r} > 1.1L_r$, $L_r > 0$ known constant bound of the uncertainty, guarantees that the sliding variable σ_r and $\dot{\sigma}_r$ defined by (28) and (29) are steered to zero in a finite time.

Proof. See [22], [46], [47].

On the sliding surface $\omega_r = \omega_{\text{opt}}$, the controlled wind turbine (1) works at the desired operating point. In the proposed procedure, the wind speed w does not have to be constant in order to compute ω_{opt}, which is tracked by ω_r of the turbine under the action of the STW controller. The control law (30) guarantees that ω_r copies the desired reference signal ω_{opt} in finite time. The convergence of the tracking error $\omega_r - \omega_{\text{opt}}$ is ensured, provided that the control gains k_{1r} and k_{2r} are chosen according to [22], [46], [47], and so to be able to counteract the effect of the drift term due to the presence of uncertainties and disturbances. STW is robust with respect to any kind of matched external disturbances and parameter variations. Therefore, even when unmodeled dynamics (e.g. shaft torsion) or mismatch of parameters (e.g. J_t, K_t) affect the turbine, the considered system can be controlled by the proposed STW (30), provided that the uncertainties act in the input channel, i.e. are matched terms, and have a bounded gradient.

Remark 1. *Let the sliding variable σ_r (28) be available to the controller affected by an unknown bounded Lebesgue-measurable noise $N(t)$. According to [22], [46], [47], the STW (30) provides for accuracy proportional to $L_r^{\frac{1}{2}}\varepsilon_r^{\frac{1}{2}}$, where $\varepsilon_r = \sup|N(t)|$.*

5 Simulation Results

As deeply described in Section 3, the optimization problem is formulated to minimize maximum $\hat{\sigma}_{T,i}$ subject to constraints on power generation in a wind farm. The output of the minimization problem is the induction factor a_i, that is related to both λ and β. The sketch of our model is in Fig. 8, in which only the optimization points (ω_{opt}, λ_{opt}) are included.

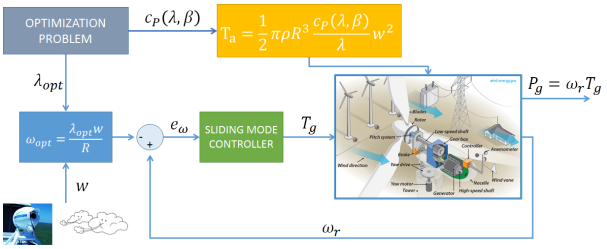

Fig. 8: Model and control of a single turbine

Two simulation scenarios are considered: (1) a diamond-shape wind farm, with equally spaced four wind turbines (see Fig. 9), and (2) four turbines of Scenario 2 in Fig. 7a, of Section 3 (see Fig. 10). For both cases, four NREL 1.5 MW turbines [7] are included. The rotor radius is $R = 35$ m and $A_0 = 3.85 \cdot 10^3$ m^2.

The coefficients of the power variation of Eq. (4) are $c_1 = 0.22$, $c_2 = 116$, $c_3 = 0.4$, $c_4 = 0.5$ and $c_5 = 12.5$. The areas of the wake interactions are evaluated as indicated in Eq. (17). The STW-SMC control system is designed with the same gains for both the points (MPPT and optimization point) and the simulation scenarios. In detail, $k_1 = 160$ and $k_2 = 15$. The simulations are performed with a Core i7-4510U CPU @2.00 GHz Processor. A fixed sample frequency of 1000 Hz, with ode4 Solver is selected to show the effectiveness of the proposed approach [48–51].

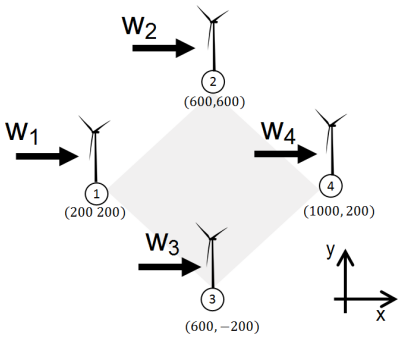

Fig. 9: Diamond shape wind farm

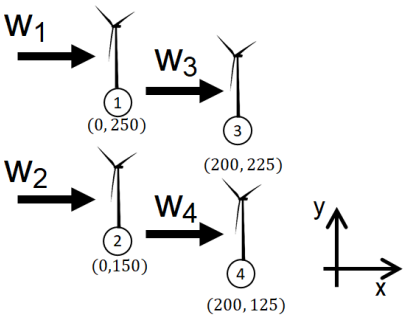

Fig. 10: Scenario 2 of optimization problem

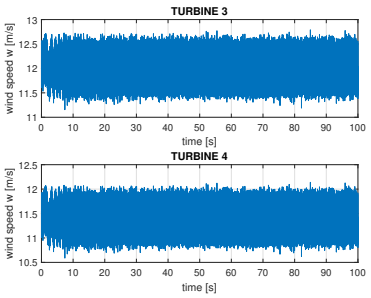

Fig. 12: Variation of the wind speed for Turbine 3 and 4 (scenario: diamond-shape)

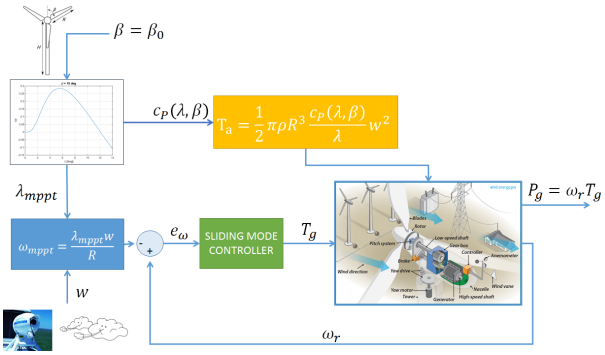

Fig. 13: Model and control of a single turbine for MPPT point

5.1 *Diamond-shape Example*

As previously said, the first scenario is a simple diamond-shape wind farm with equally spaced turbines, in which only Turbine 4 is affected by the other turbines and its wind speed is significantly reduced due to wake interactions. The areas of the wake interactions are evaluated as indicated in Eq. (17). For example, if the second turbine is analyzed, $R(x_{12}) = R + \alpha x_{12}$, with $\alpha = 0.05$ and $x_{12} = |x_1 - x_2| = 400$ m. From $R(x_{12})$, it is possible to evaluate all the parameters in Eq. (18). $A_{sh_{12}}$ is the shadowed area between Turbine 1 and 2 and is considered equal to 0. This means that no aerodynamic interactions are considered between the two turbines, due to the layout of the wind farm. For the turbine 4, which is affected by the wake model, $R(x_{14}) = R + \alpha x_{14}$, with $\alpha = 0.05$ and $x_{14} = |x_1 - x_4| = 800$ m. $A_{sh_{14}}$ is the shadowed area between Turbine 1 and 4 and is considered equal to A_0 ($= 3.85 \cdot 10^3$ m^2). This shadowed area is different from zero value because the Turbine 4 is strongly affected by the other turbines.

A simulation of 100 s is performed, with a variation of the wind speed as in Figs. 11 and 12, which the average value is . As described above, we assume that the wind speed is measured with a LIDAR sensor placed in the first turbine and that the wind speed acting on the other turbines is evaluated with Jensen wake model. The measurements are affected by a random noise, simulating the noise of the sensor itself.

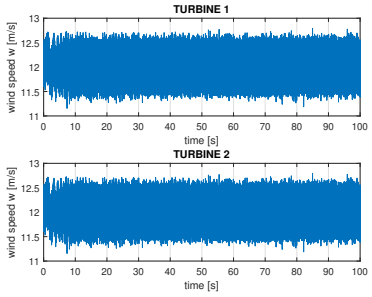

Fig. 11: Variation of the wind speed for Turbine 1 and 2 (scenario: diamond-shape)

5.1.1 MPPT Tracking Results: The proposed control scheme for a single turbine (for example, turbine 1) is reported in Fig. 13. The SMC is designed for the control of the rotor speed ω_r and the pitch angle β is supposed as a constant.

As indicated in Section 2, the optimum angular speed ω_{mppt} is function of the variable wind speed and of the optimal tip-speed ratio, according to $\omega_{\text{mppt}} = \lambda_{\text{mppt}} w/R$, and in the wind farm it varies in accordance to the variation of the wind speed and of the λ_{mppt}. With a fixed β, first we evaluate the maximum tip-speed ratio by an iterative process. The axial induction factors for the MPPT case are $a = 0.1525$, for all the turbines and these determine turbulence intensity factors as

$$I_{\text{eff},1} = 0.0341, \qquad I_{\text{eff},2} = 0.0447,$$
$$I_{\text{eff},3} = 0.0421, \qquad I_{\text{eff},4} = 0.0346.$$

The tip-speed ratio $\lambda_{\text{mppt}} = 6.3206$ is obtained as the peak of power coefficient (see Fig. 2, with fixed $\beta = 0$ deg). After the definition of these parameters, the optimum angular speed for each wind turbines is

$$\omega_{\text{mppt},i} = \frac{\lambda_{\text{mppt}} w_i}{R},$$

where w_i is the wind speed evaluated with the wake model (as described in Section 2.3) for the i-th turbine and R is the radius of the i-th turbine. In the selected wind farm configuration, all the turbines have the same radius, $R = 35$ m, and are equally spaced.

As previously said, the aerodynamic interactions concern only the turbine 4, the input of which is a reduced wind speed. For the MPPT case, it is assumed that the axial factor is the same for all the turbines, therefore maximum power extraction is guaranteed.

For this case, the maximum total power produced by the wind farm is $P_{g,\text{mppt}} = 7.191 \cdot 10^6$ W and the maximum fatigue value is $F_{\text{max,mppt}} = \sum_{i=1}^{n} F_i = 2.899 \cdot 10^6$ N.

The error of the angular velocity of the turbine, that is controlled by the SMC controller, is about $e_{\omega,mppt} = 2.268 \cdot 10^{-5}$ rad/s $\simeq 2.166 \cdot 10^{-4}$ rpm after 100 seconds of simulation, as in Table 1.

5.1.2 Fatigue Reduction Tracking Results: The main objective of the proposed combination of control system and optimization problem is the reduction of the fatigue value of a wind farm, in which aerodynamic interactions are included. The proposed optimization problem is able to reduce the fatigue, so the maintenance costs of a wind farm, with a good power extraction. The axial induction factors obtained by the optimization problem and corresponding tip-speed ratios and pitch angles were

$$a_1 = 0.1330, \quad a_2 = 0.1481, \quad a_3 = 0.1107, \quad a_4 = 0.1256,$$
$$\lambda_1 = 5.0652, \quad \lambda_2 = 5.7244, \quad \lambda_3 = 4.4594, \quad \lambda_4 = 4.8424,$$

$$\beta_i = 0, \quad i = 1, 2, 3, 4.$$

As previously stated, the maximum value of the axial factor is $a_{\text{mppt}} = 0.1525$, which corresponds to the maximum value that can be reached by the selected turbine.

The maximum value of fatigue for the optimized problem is $F\text{max, opt} = \sum_{i=1}^{n} F_i = 2.523 \cdot 10^6$ N, with a loss of fatigue loads of about 13% with respect to the MPPT case. Turbulence intensity factors are

$$I_{\text{eff},1} = 0.0324, \qquad I_{\text{eff},2} = 0.0410,$$
$$I_{\text{eff},3} = 0.0410, \qquad I_{\text{eff},4} = 0.0330.$$

Moreover, power extraction is reduced and in the analyzed case we have a reduction of the total power generated by about 8%. In detail, the maximum produced power is $P_{g,\text{opt}} = 6.668 \cdot 10^6$ W. In Fig. 15 it is possible to observe a damage reduction of more than 80%. The total power produced is compared with the power extracted tracking the MPPT point for a simulation of 100 seconds. As in Fig. 16, the difference of the extracted power is not so high, compared to the high reduction of fatigue that is guaranteed with the proposed approach. The STW-SMC control system is able to track the optimized angular velocity, i.e. the angular velocity obtained with the optimization problem, as in the previous case. The error of the angular velocity is evaluated for the first turbine and it is about $e_{\omega,opt} = 7.119 \cdot 10^{-5}$ rad/s $\simeq 6.80 \cdot 10^{-4}$ rpm at the end of simulation. Similar values are obtained by the other turbines as in Table 1.

Table 1 Error of the angular velocity for the Diamond-shape scenario

Operating point	Turbine #	Error e_ω [rpm]
MPPT Diamond-shape	1	$2.166 \cdot 10^{-4}$
MPPT Diamond-shape	2	$2.166 \cdot 10^{-4}$
MPPT Diamond-shape	3	$2.166 \cdot 10^{-4}$
MPPT Diamond-shape	4	$2.171 \cdot 10^{-4}$
Fatigue Diamond-shape	1	$6.80 \cdot 10^{-4}$
Fatigue Diamond-shape	2	$2.12 \cdot 10^{-4}$
Fatigue Diamond-shape	3	$7.72 \cdot 10^{-5}$
Fatigue Diamond-shape	4	$7.48 \cdot 10^{-5}$

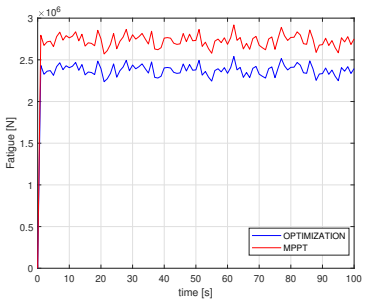

Fig. 14: Comparison of fatigue value $F = \sum_{i=1}^{4} F_i$ between MPPT case and the optimized problem (scenario: diamond-shape)

5.2 Four turbines scenario

The second scenario, as previously said, is a wind farm with four turbines as in Fig. 10. As in the previous case, a simulation of 100 s is performed, with a fixed-step sample frequency of 1000 Hz and ode4 solver.

The average wind speed applied to the wind farm is 12 [m/s] and the variation of this speed is in Figs. 17 and 18. As for the previous case, the wind speed of the first two turbines is measured by a

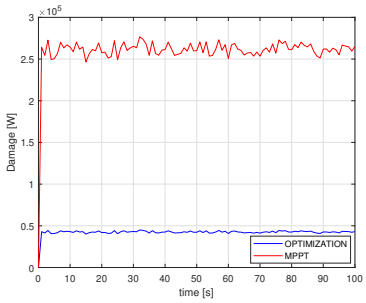

Fig. 15: Comparison of damage $D = \sum_{i=1}^{4} D_i$ between MPPT case and the optimized problem (scenario: diamond-shape)

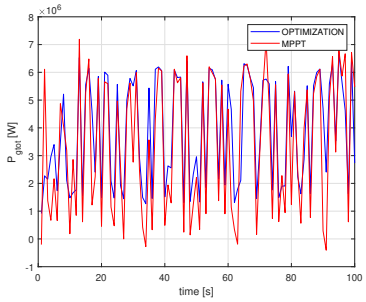

Fig. 16: Comparison of extracted power between MPPT case and the optimized problem (scenario: diamond-shape)

LIDAR sensor, instead, for this wind farm configuration, both the turbine 3 and 4 are affected by the wake interactions. Moreover, the wake interactions are evaluated as in Eq. (17).

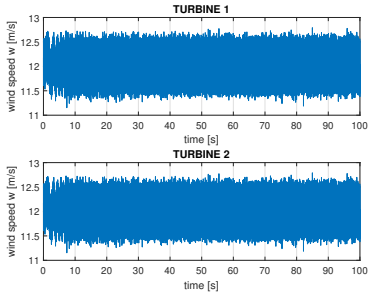

Fig. 17: Variation of the wind speed for Turbine 1 and 2 (scenario 2: four turbines)

5.2.1 MPPT Tracking Results: The MPPT solution is the same as the diamond-shape, with and induced axial factor of $a = 0.1525$ for all the turbines, tip-speed ration $\lambda = 6.3026$, and a fixed pitch angle $\beta = 0$ deg. The optimum angular speed ω_{mppt} has the same value of the previous example.

For this case, the maximum total power produced by the wind farm is $P_{g,\text{mppt}} = 6.612 \cdot 10^6$ W, turbulence intensity factors are $I_{\text{eff},1} = 0.0926$, $I_{\text{eff},3} = 0.0934$, and $I_{\text{eff},2} = 0.0934$, $I_{\text{eff},4} = 0.0926$, and the maximum fatigue value is $F_{\text{max,mppt}} = \sum_{i=1}^{n} F_i = 2.878 \cdot 10^6$ N.

5.2.2 Fatigue Reduction Tracking Results: For the fatigue reduction tracking, the main objective, as before, is the combination of the control system and the optimizations problem for the fatigue evaluation, including aerodynamic interactions. The axial factors and the effective turbulence intensity are evaluated with an optimization problem, including only 4 turbines (as in Fig. 10). When we consider the second scenario with $w_\infty = 12$ m/s and $P_d = 1.8$ MW,

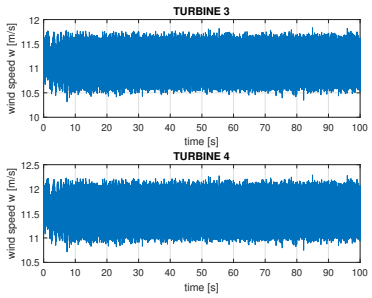

Fig. 18: Variation of the wind speed for Turbine 3 and 4 (scenario 2: four turbines)

we obtained

$$
\begin{aligned}
a_1 &= 0.1177, \quad a_3 = 0.1225, \\
a_2 &= 0.1225, \quad a_4 = 0.1177, \\
I_{\text{eff},1} &= 0.0865, \quad I_{\text{eff},3} = 0.0865, \\
I_{\text{eff},2} &= 0.0865, \quad I_{\text{eff},4} = 0.0865, \\
\lambda_1 &= 4.6315, \quad \lambda_3 = 4.7576, \\
\lambda_2 &= 4.7576, \quad \lambda_4 = 4.6318, \\
\beta_i &= 0, \quad i = 1, 2, 3, 4.
\end{aligned}
$$

For the turbines 1 and 2, we assume that $w_1 = w_2 = w_\infty$ (as in Fig. 10), so no wake interactions are analyzed. The shadowing areas are evaluated as in the previous Section. For example, for turbine 3, which is affected by the wake model, we consider the interactions with turbine 2 and we have $R(x_{23}) = R + \alpha x_{23}$ with $\alpha = 0.05$ and $x_{23} = |x_2 - x_3| = 200$ m. The symbol $A_{sh_{13}}$ is the shadowed area between Turbine 1 and 3 and is considered equal to $1.561 \cdot 10^3$ m^2. This shadowed area is different from zero value because the Turbine 3 is affected by the other turbines, and, in detail, is affected by the turbine 2.

The maximum value of fatigue for the optimized problem is $F_{\text{max,opt}} = \sum_{i=1}^{n} F_i = 2.353 \cdot 10^6$ N, with a loss of fatigue of about 18% with respect to the MPPT case.

As previously stated, power extraction is reduced and in the analyzed case we have a reduction of the total generated power of about 4%. In detail, the maximum produced power is $P_{g,\text{opt}} = 6.410 \cdot 10^6$ W. In Fig. 20 it is possible to observe a damage reduction of about 24%. The total produced power is compared with the power extracted tracking the MPPT point for a simulation of 100 seconds. As in Fig. 21, the difference of the extracted power is not so high, compared to the reduction of fatigue, that is guaranteed with the proposed approach. The error of the angular velocity is evaluated for the first turbine at the end of simulation and it is about $e_{\omega,mppt} = 4.74 \cdot 10^{-6}$ rad/s $\simeq 4.53 \cdot 10^{-5}$ rpm.

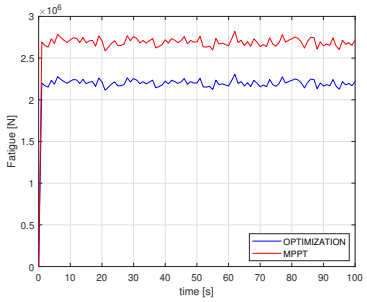

Fig. 19: Comparison of fatigue value $F = \sum_{i=1}^{4} F_i$ between MPPT case and the optimized problem (scenario 2: four turbines)

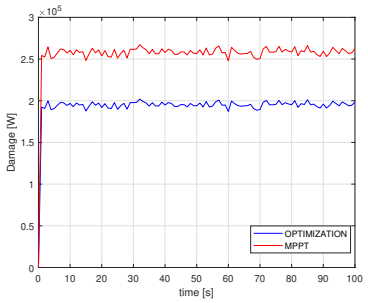

Fig. 20: Comparison of damage $D = \sum_{i=1}^{4} D_i$ between MPPT case and the optimized problem (scenario 2: four turbines)

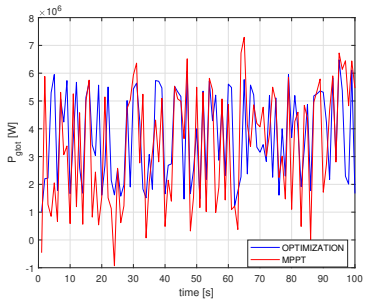

Fig. 21: Comparison of extracted power between MPPT case and the optimized problem (scenario 2: four turbines)

The STW-SMC control system is able to track the angular velocity obtained with the optimization problem, as in the previous case. The error of the angular velocity is evaluated for the first turbine at the end of simulation and it is about $e_{\omega,opt} = 8.922 \cdot 10^{-6}$ rad/s $\simeq 8.52 \cdot 10^{-5}$ rpm. Similar values are obtained by the other turbines as in Table 2.

Table 2 Error of the angular velocity for the Scenario 2

Operating point	Turbine #	Error e_ω [rpm]
MPPT Scenario	1	$4.53 \cdot 10^{-5}$
MPPT Scenario	2	$4.53 \cdot 10^{-5}$
MPPT Scenario	3	$4.53 \cdot 10^{-5}$
MPPT Scenario	4	$4.196 \cdot 10^{-5}$
Fatigue Scenario	1	$8.52 \cdot 10^{-5}$
Fatigue Scenario	2	$8.442 \cdot 10^{-5}$
Fatigue Scenario	3	$8.731 \cdot 10^{-5}$
Fatigue Scenario	4	$8.68 \cdot 10^{-5}$

Finally, in Table 3 the results, obtained for all the cases, are summarized.

Table 3 Summary of the simulation results

Scenario	Power [W]	Fatigue [N]	Damage [-]
MPPT Diamond-shape	$7.191 \cdot 10^6$	$2.899 \cdot 10^6$	$2.747 \cdot 10^5$
Fatigue Diamond-shape	$6.668 \cdot 10^6$	$2.523 \cdot 10^6$	$4.469 \cdot 10^4$
MPPT Scenario 2	$6.612 \cdot 10^6$	$2.878 \cdot 10^6$	$2.703 \cdot 10^5$
Fatigue Scenario 2	$6.410 \cdot 10^6$	$2.353 \cdot 10^6$	$2.063 \cdot 10^5$

6 Concluding Remarks

Wind farm scenarios are analyzed in this paper, including interference raising among the wind turbines. An optimization problem is defined with the aim to find the operational points for the turbines in

the wind farm such that maximum fatigue risk among the turbines is minimized subject to a generation power constraint. The operating points of the wind turbine are used for the tracking of the rotor angular velocity, provided by a Sliding Mode Controller (SMC). A minimization of the fatigue loads with a minimum loss of power extraction is shown for two different scenarios. For both cases, the optimization problem guarantees that the reduction of power extraction is low compared to the reduction of damage and fatigue. This trade-off can guarantee a reduction of maintenance costs, without compromising the power extraction. Moreover, a good tracking of the angular velocity is obtained with the proposed second order SMC. Future works will include the model of doubly-fed induction generator (DFIG) and mechanical stresses, to show the effectiveness of the proposed control strategy.

Acknowledgment

This work was supported by COOPS, International Bilateral Joint CNR Laboratories, and JST CREST Grant Number JPMJCR15K2, Japan.

7 References

1 Pao, L.Y., Johnson, K.E.: 'Control of wind turbines', *IEEE Control Systems Magazine*, 2011, **31**, (2), pp. 44–62
2 Fagiano, L., Morari, M., Rotea, M., Stewart, G.: 'Editorial to tame the wind: Advanced control applications in wind energy', *IEEE Transactions on Control Systems Technology*, 2013, **21**, (4), pp. 1045–1048
3 Nguyen, H.M., Naidu, D.S. In: 'Evolution of wind turbine control systems,'. (Encyclopedia of Control Systems, Robotics, and Automation; EOLSS Publishers: Oxford, UK, 2010.
4 Soleimanzadeh, M., Wisniewski, R., Kanev, S.: 'An optimization framework for load and power distribution in wind farms', *Journal of Wind Engineering and Industrial Aerodynamics*, 2012, **107**, pp. 256–262
5 Jensen, N.O. 'A note on wind generator interaction'. (Risø National Laboratory for Sustainable Energy, Technical University of Denmark, 1983.
6 van Wingerden, J.W., Pao, L., Aho, J., Fleming, P.: 'Active power control of waked wind farms', *IFAC-PapersOnLine*, 2017, **50**, (1), pp. 4484 – 4491. 20th IFAC World Congress
7 Pao, L.Y., Johnson, K.E. 'A tutorial on the dynamics and control of wind turbines and wind farms'. In: 2009 American Control Conference. (, 2009. pp. 2076–2089
8 Boersma, S., Doekemeijer, B.M., Gebraad, P.M.O., Fleming, P.A., Annoni, J., Scholbrock, A.K., et al. 'A tutorial on control-oriented modeling and control of wind farms'. In: 2017 American Control Conference (ACC). (, 2017. pp. 1–18
9 Heer, F., Esfahani, P.M., Kamgarpour, M., Lygeros, J. 'Model based power optimisation of wind farms'. In: 2014 European Control Conference. (, 2014. pp. 1145–1150
10 Al, F., Abdulsada, M., Abusief, F.: 'Speed control of wind turbine by using pid controller', *Engineering and Technology Journal*, 2009, **29**, (1), pp. 65–71
11 Ahmed, O.A., AwadAhmed, A.: 'Control of wind turbine for variable speed based on fuzzy-pid controller', *SUST Journal of Engineering and Computer Sciences*, 2016, **18**, (1)
12 Jafarnejadsani, H., Pieper, J., Ehlers, J.: 'Adaptive control of a variable-speed variable-pitch wind turbine using radial-basis function neural network', *IEEE Transactions on Control Systems Technology*, 2013, **21**, (6), pp. 2264–2272
13 Jabbari.Asl, H., Yoon, J.: 'Adaptive control of variable-speed wind turbines for power capture optimisation', *Transactions of the Institute of Measurement and Control*, 2017, **39**, (11), pp. 1663–1672
14 De.Corcuera, A.D., Pujana.Arrese, A., Ezquerra, J.M., Segurola, E., Landaluze, J.: 'H_∞ based control for load mitigation in wind turbines', *Energies*, 2012, **5**, (4), pp. 938–967
15 Han, Y., Leithead, W.: ; IOP Publishing. 'Combined wind turbine fatigue and ultimate load reduction by individual blade control', *Journal of physics: Conference series*, 2014, **524**, (1), pp. 012062
16 Yuan, Y., Tang, J.: 'On advanced control methods toward power capture and load mitigation in wind turbines', *Engineering*, 2017, **3**, (4), pp. 494–503
17 Evangelista, C., Puleston, P., Valenciaga, F., Fridman, L.M.: 'Lyapunov-Designed Super-Twisting Sliding Mode Control for Wind Energy Conversion Optimization', *IEEE Transactions on Industrial Electronics*, 2013, **60**, (2), pp. 538–545
18 Beltran, B., Ahmed.Ali, T., Benbouzid, M.E.H.: 'High-order sliding-mode control of variable-speed wind turbines', *IEEE Transactions on Industrial electronics*, 2009, **56**, (9), pp. 3314–3321
19 Barambones, O., Gonzalez de Durana, J.M. 'Wind turbine control scheme based on adaptive sliding mode controller and observer'. In: 2015 IEEE 20th Conference on Emerging Technologies Factory Automation. (, 2015. pp. 1–7
20 Gajewski, P., Pieńkowski, K. 'Analysis of sliding mode control of variable speed wind turbine system with pmsg'. In: 2017 International Symposium on Electrical Machines. (, 2017. pp. 1–6
21 Hong, C.M., Huang, C.H., Cheng, F.S.: 'Sliding mode control for variable-speed wind turbine generation systems using artificial neural network', *Energy Procedia*, 2014, **61**, pp. 1626 – 1629. international Conference on Applied Energy, ICAE2014
22 Levant, A.: 'Sliding order and sliding accuracy in sliding mode control', *International journal of control*, 1993, **58**, (6), pp. 1247–1263
23 Gualtieri, G.: 'A novel method for wind farm layout optimization based on wind turbine selection', *Energy Conversion and Management*, 2019, **193**, pp. 106–123
24 González, J.S., Rodriguez, A.G.G., Mora, J.C., Santos, J.R., Payan, M.B.: 'Optimization of wind farm turbines layout using an evolutive algorithm', *Renewable energy*, 2010, **35**, (8), pp. 1671–1681
25 Capello, E., Wada, T., Punta, E., Fujisaki, Y. 'Minimax optimization of fatigue loads in a wind farm and its realization via sliding mode controller of wind turbines'. In: 2018 IEEE Conference on Control Technology and Applications (CCTA). (, 2018. pp. 430–435
26 Capello, E., Wada, T., Punta, E., Fujisaki, Y. 'Wind farm sliding mode control and energy optimization with fatigue constraints'. In: SICE International Symposium on Control Systems 2018. (, 2018. pp. Sa23–5
27 Jensen, T.N., Knudsen, T., Bak, T.: ; IOP Publishing. 'Fatigue minimising power reference control of a de-rated wind farm', *Journal of Physics: Conference Series*, 2016, **753**, (5), pp. 052022
28 Johnson, K.E. 'Adaptive torque control of variable speed wind turbines'. (National Renewable Energy Laboratory, 2004.
29 Beltran, B., Ahmed.Ali, T., Benbouzid, M.E.H.: 'Sliding mode power control of variable-speed wind energy conversion systems', *IEEE Transactions on energy conversion*, 2008, **23**, (2), pp. 551–558
30 Lang, S., McKeogh, E.: 'Lidar and sodar measurements of wind speed and direction in upland terrain for wind energy purposes', *Remote Sensing*, 2011, **3**, (9), pp. 1871–1901
31 Bao, J., Yue, H., Leithead, W.E., Wang, J.Q.: 'Feedforward control for wind turbine load reduction with pseudo-lidar measurement', *International Journal of Automation and Computing*, 2018, **15**, (2), pp. 142–155
32 Heier, S.: 'Grid Integration of Wind Energy Conversion Systems'. (Wiley, 1998)
33 Rosyadi, M., Muyeen, S.M., Takahashi, R., Tamura, J. 'Stabilization of fixed speed wind generator by using variable speed pm wind generator in multi-machine power system'. In: 2012 15th International Conference on Electrical Machines and Systems. (, 2012. pp. 1–6
34 Safari, B.: 'Modeling wind speed and wind power distributions in rwanda', *Renewable and Sustainable Energy Reviews*, 2011, **15**, (2), pp. 925–935
35 Johnson, W.: 'Helicopter Theory'. (Dover, 1980)
36 Jenkins, N., Burton, A., Sharpe, D., Bossanyi, E. 3. In: 'Aerodynamics of horizontal-axis wind turbines'. (John Wiley & Sons, Ltd, 2002. pp. 41–172
37 Horvat, T., Spudić, V., Baotić, M. 'Quasi-stationary optimal control for wind farm with closely spaced turbines'. In: 2012 Proceedings of the 35th International Convention MIPRO. (, 2012. pp. 829–834
38 Ragheb, M., Ragheb, A.M. 'Wind turbines theory-the betz equation and optimal rotor tip speed ratio'. In: Fundamental and advanced topics in wind power. (InTech, 2011.
39 Sorensen, P., Andresen, B., Bech, J., Fortmann, J., Pourbeik, P. 'Progress in iec 61400-27 electrical simulation models for wind power generation'. In: Proceedings of the 11th International Workshop on Large-Scale Integration of Wind Power into Power Systems as well as on Transmission Networks for Offshore Wind Power Plants. (, 2012.
40 Frandsen, S., Thøgersen, M.L.: 'Integrated fatigue loading for wind turbines in wind farms by combining ambient turbulence and wakes', *Wind Engineering*, 1999, pp. 327–339
41 Barradas-Berglind, J.J., Wisniewski, R. 'Wind farm axial-induction factor optimization for power maximization and load alleviation'. In: 2016 European Control Conference (ECC). (, 2016. pp. 891–896
42 González.Longatt, F., Wall, P., Terzija, V.: 'Wake effect in wind farm performance: Steady-state and dynamic behavior', *Renewable Energy*, 2012, **39**, (1), pp. 329–338
43 Spellucci, P.: 'A new technique for inconsistent qp problems in the sqp method', *Journal of Mathematical Methods of Operations Research*, 1998, **47**, (3), pp. 355–400
44 Byrd, R.H., Hribar, M.E., Nocedal, J.: 'An interior point algorithm for large-scale nonlinear programming', *SIAM Journal on Optimization*, 1999, **9**, (4), pp. 877–900
45 Shtessel, Y., Edwards, C., Fridman, L., Levant, A.: 'Sliding mode control and observation'. (Springer Science+Business Media, New York, 2014)
46 Levant, A.: 'Universal single-input–single-output (siso) sliding-mode controllers with finite-time convergence', *IEEE Transactions on Automatic Control*, 2001, **46**, (9), pp. 1447–1451
47 Levant, A.: 'Quasi-continuous high-order sliding-mode controllers', *IEEE Transactions on Automatic Control*, 2005, **50**, (11), pp. 1812–1816
48 Gear, C.W., Osterby, O.: 'Solving Ordinary Differential Equations with Discontinuities', *ACM Transactions on Mathematical Software*, 1984, **10**, (1), pp. 23–44
49 Calvo, M., Montijano, J.I., Rández, L.: 'On the solution of discontinuous IVPs by adaptive Runge-Kutta codes', *Numerical Algorithms*, 2003, **33**, (1-4), pp. 163–182
50 Dieci, L., Lopez, L.: 'A survey of numerical methods for IVPs of ODEs with discontinuous right-hand side', *Journal of Computational and Applied Mathematics*, 2012, **236**, (16), pp. 3967–3991
51 Dieci, L., Lopez, L.: 'Numerical solution of discontinuous differential systems: Approaching the discontinuity surface from one side', *Applied Numerical Mathematics*, 2013, **67**, pp. 98–110
52 Jenkins, N., Burton, A., Sharpe, D., Bossanyi, E.: 'Wind Energy Handbook'. (Wiley, 2001)
53 Gebraad, P., Van.Wingerden, J.: 'Maximum power-point tracking control for wind farms', *Wind Energy*, 2015, **18**, (3), pp. 429–447
54 Kulunk, E. 'Aerodynamics of wind turbines'. In: Fundamental and Advanced Topics in Wind Power. (InTech, 2011.
55 Peña, A., Réthoré, P.E., van der Laan, M.P.: 'On the application of the jensen wake model using a turbulence-dependent wake decay coefficient: the sexbierum case', *Wind Energy*, 2016, **19**, (4), pp. 763–776

56 Slootweg, J.G., Polinder, H., Kling, W.L. 'Dynamic modelling of a wind turbine with doubly fed induction generator'. In: 2001 Power Engineering Society Summer Meeting. Conference Proceedings (Cat. No.01CH37262). (IEEE, 2001. pp. 644–649

57 Thakar, P.S., Bandyopadhyay, B., Gandhi, P.: 'Improved output-feedback second order sliding mode control design with implementation for underactuated slosh-container system having confined track length', *IET Control Theory & Applications*, 2016, **11**, (8), pp. 1316–1323